Bacteria activate sensory neurons that modulate pain and inflammation

Published in final edited form as:
Nature. 2013 September 5; 501(7465): 52–57. doi:10.1038/nature12479.

Bacteria activate sensory neurons that modulate pain and inflammation

Isaac M. Chiu[1], **Balthasar A. Heesters**[2,3], **Nader Ghasemlou**[1], **Christian A. Von Hehn**[1], **Fan Zhao**[4], **Johnathan Tran**[1], **Brian Wainger**[1], **Amanda Strominger**[1], **Sriya Muralidharan**[1], **Alexander R. Horswill**[5], **Juliane Bubeck Wardenburg**[6], **Sun Wook Hwang**[1,7], **Michael C. Carroll**[2], and **Clifford J. Woolf**[1]

[1]Kirby Neurobiology Center, Boston Children's Hospital, and Department of Neurobiology, Harvard Medical School, Boston, Massachusetts 02115, USA. [2]Boston Children's Hospital, Program in Cellular and Molecular Medicine, and Harvard Medical School, Boston, Massachusetts 02115, USA. [3]Medical Microbiology, University Medical Center, Utrecht, Utrecht, The Netherlands. [4]Department of Chemistry, Quantitative Biology Program, Brandeis University, Waltham, Massachusetts 02454, USA. [5]Department of Microbiology, Roy J. and Lucille A. Carver College of Medicine, University of Iowa, Iowa City, Iowa 52242, USA. [6]Departments of Pediatrics and of Microbiology, University of Chicago, Chicago, Illinois 60637, USA. [7]Korea University Graduate School of Medicine, Seoul 136-705, Korea.

Summary

Nociceptor sensory neurons are specialized to detect potentially damaging stimuli, protecting the organism by initiating the sensation of pain and eliciting defensive behaviors. Bacterial infections produce pain by unknown molecular mechanisms, although they are presumed secondary to immune activation. Here we demonstrate that bacteria directly activate nociceptors, and that the immune response mediated through TLR2, MyD88, T cells, B cells, and neutrophils/monocytes is not necessary for *Staphylococcus aureus* induced pain in mice. Mechanical and thermal hyperalgesia parallels live bacterial load rather than tissue swelling or immune activation. Bacteria induce calcium flux and action potentials in nociceptor neurons, in part via bacterial N-formylated peptides and the pore-forming toxin alpha-hemolysin through distinct mechanisms. Specific ablation of Nav1.8-lineage neurons, which include nociceptors, abrogated pain during bacterial infection, but concurrently increased local immune infiltration and lymphadenopathy of the draining lymph node. Thus, bacterial pathogens produce pain by directly activating sensory neurons that modulate inflammation, an unsuspected role for the nervous system in host-pathogen interactions.

Corresponding author: Clifford J. Woolf, clifford.woolf@childrens.harvard.edu.

Author contributions and accession numbers

IMC, CJW designed the study. IMC, BAH-infection and immune analysis. IMC, NG-behavioral analysis. NG, AS-cytokine profiling. IMC, SM-microscopy. IMC, CAV, JT-neuronal culture, calcium imaging. SWH-electrophysiology. FZ-peptide synthesis and chemistry. BW-multielectrode arrays. JBW, ARH generated bacterial strains. JBW-recombinant Hla. JBW, MCC, CJW-supervision and expertise. IMC, CJW wrote the manuscript. Microarray data are deposited at NCBI GEO database (accession no. GSE46546).

Authors declare no competing financial interests.

Supplemental Information

Supplemental methods and figures are available online at www.nature.com/nature.

Introduction

A dense network of low and high threshold sensory nerves innervate peripheral tissues including the skin, respiratory, and gastrointestinal tracts, which are often exposed to bacterial pathogens. Bacterial infection induces inflammation through immune cell recruitment[1]. Inflammatory pain during infection has been thought to be triggered by the action of immune-derived proteins (e.g. cytokines and growth factors), lipids (e.g. prostaglandins), and other mediators like amines, potassium, and protons on receptors expressed by nociceptors[2,3].

S. aureus is a major cause of wound and surgical infections, leading to painful abscesses, cellulitis, necrotizing fascitis[4,5]. *S. aureus* releases toxins including hemolysins, Panton-Valentine Leukocidin (PVL), and phenol soluble modulins, which play roles in bacterial dissemination and tissue damage[6,7,8]. We have now investigated the molecular mechanisms of pain generation during *S. aureus* infection. Unexpectedly, key immune activation pathways were not necessary for hyperalgesia during acute infection. Rather, bacteria directly activated nociceptors through N-formyl peptides and the pore-forming toxin alpha-hemolysin (Hla). Moreover, we find that nociceptors release neuropeptides that modulate innate immune activation during infection.

Pain correlates with bacterial load

To study the nature of pain caused by bacterial pathogens, we established a *S. aureus* infection model of the mouse hind-paw. Subcutaneous injection of LAC/USA300 (5×10^6 CFU), a community associated-methicillin resistant *S. aureus* strain (CA-MRSA)[8,9] resulted in mechanical, heat, and cold hypersensitivity within one hour that lasted for 48-72 hours (Fig. 1a). This hyperalgesia peaked at 6 hours post-infection, and began to decrease at 24 hours.

We quantified the kinetics of tissue swelling, immune activation, and bacterial clearance. Tissue swelling did not correlate with pain, but showed an immediate peak following bacterial injection, and a second peak at 48 hours post-infection (Fig. 1a). Using flow cytometry, we found increases in myeloid immune cells in infected tissues ($CD11b^+CD45^+$; Fig. 1b), constituted primarily of $Ly6G^+$ neutrophils and $Ly6C^{lo}$ monocytes, with fewer $Ly6C^{hi}$ monocytes (Supplemental Fig. 1, Fig. 1b). This influx began at 6 hours, with a peak at 48 hours post-infection and a reduction at 72 hours (Fig. 1b). KC and MCP-1, chemokines that mediate neutrophil/monocyte recruitment, peaked early (Supplemental Fig. 2), while TNF-α and IL-1β, pro-inflammatory cytokines which directly sensitize nociceptors[10,11], also increased in infected tissue but did not correlate with hyperalgesia (Fig. 1c).

We next analyzed live bacterial load in infected tissues. *S. aureus* recovery peaked at 6 hours, and then decreased over time, similar to the time-course of pain hypersensitivity (Fig. 1d). This decrease was accompanied by myeloid cell ingestion of bacteria, as detected by flow cytometry (Supplemental Fig. 1). In infected Nav1.8-Cre/TdTomato reporter mice, *S. aureus* (GFP-USA300) were often found in close proximity to dermal but not epidermal nociceptor fibers (Fig. 1e, Supplemental Fig. 3), suggesting potential direct nerve-bacteria interactions. Taken together, hyperalgesia mirrors the time-course of bacterial expansion and not tissue swelling or immune activation (Diagram, Supplemental Fig. 4).

Innate and adaptive host defenses not necessary for *S. aureus* pain

We determined whether key immune response pathways were necessary for *S. aureus* induced pain. Innate immune cells recognize *S. aureus* derived cell-wall components through TLR2[12], leading to NF-κB activation through adaptor Myeloid differentiation factor

88 (MyD88). TLR2/MyD88 protect mice against *S. aureus* skin infection[4,13]. TLR3, 4, 7, and 9 are also functional expressed in sensory neurons[14,15]. Thus, we analyzed pain responses in TLR2$^{-/-}$ and MyD88$^{-/-}$ mice following *S. aureus* infection. Surprisingly, mechanical and thermal hyperalgesia were not reduced in these mice (Fig. 2a, Supplemental Fig. 5). At 72 hours, MyD88$^{-/-}$ mice showed elevated hypersensitivity, which may reflect greater bacterial load due to reduced immune activation and bacterial clearance (Fig. 2a-b).

Neutrophils and monocytes are circulating leukocytes critical for innate immunity against *S. aureus*, rapidly infiltrating sites of infection to limit pathogen survival and spread[4, 16]. We treated mice with GR1 antibody prior to infection, which eliminated blood-borne and splenic neutrophils and monocytes (Supplemental Fig. 6). Plantar tissue-infiltrating neutrophils and monocytes during *S. aureus* infection were completely depleted by GR1 (Supplemental Fig. 7; reduction of 97% of all CD45^{+} immune cells in infected tissues). However, instead of lessening hyperalgesia, GR1 depletion significantly increased mechanical and heat hypersensitivity (Fig. 2c). This was accompanied by higher bacterial load, reflecting the key role of these myelomonocytic cells in combating *S. aureus* (Fig. 2d). We repeated the experiment using injection of heat-killed (hk) *S. aureus* (10^8 CFU), and found that GR1 treatment decreased tissue swelling, but did not affect pain-like hypersensitivity (Supplemental Fig. 8). The increased pain during *S. aureus* infection following GR1 depletion is likely linked to uncontrolled bacterial expansion (Fig. 2d), but may also reflect neutrophil analgesic factors[17].

To further analyze the contribution of the immune system to pain, we examined *S. aureus* infection in Nod.scid.gamma mice, which are deficient in natural killer, T, and B cells[18]. Infection-induced mechanical and heat hyperalgesia did not differ between Nod.scid.gamma and Nod.WT mice (Supplemental Fig. 9). To control for strain-dependent differences, we also analyzed C57BL/6 congenic RAG1$^{-/-}$ mice, which are deficient in mature T and B cells[19]. Pain-like hypersensitivity did not differ following *S. aureus* infection in B6.RAG1$^{-/-}$ mice compared to B6.WT mice (Supplemental Fig. 9). Based on these results, we conclude that adaptive immunity through T and B cells is not required for acute bacterial pain.

Formyl peptides and α-hemolysin activate nociceptors

The strong correlation between pain and bacterial load suggested that nociceptors directly interact with bacteria during pathogen invasion. To test this, we applied hk-bacteria on dorsal root ganglia (DRG) sensory neurons. Hk-*S. aureus* induced a robust calcium flux response in a subset of neurons that also responded to capsaicin, which activates transient receptor potential V1 (TRPV1) (Fig. 3a). Hk-*S. aureus* application also induced action potential firing in capsaicin-responsive DRG neurons (Fig. 3b). Extending these results, we found that several other strains of hk-bacteria caused calcium flux in DRG neurons (Fig. 3c, responsive cells: hk-*S. aureus*=152/1046, hk-*S. pneumoniae*=82/968, hk-*L. monocytogenes*=67/852, hk-*M. fermentans*=9/339, hk-*H. pylori*=85/1365, hk-*P. aeruginosa*=14/269, hk-*E. coli*=3/233). Nav1.8-Cre/TdTomato reporter mice were used to genetically mark nociceptors[20] and all bacteria-evoked neuronal responses were within the Nav1.8-Cre/TdTomato^{+} population (Supplemental Fig. 10). Patterns of nociceptor responsiveness to particular bacteria differed, suggesting strain-specific ligands acting through disparate mechanisms (Supplemental Fig. 11). Intraplantar injection of different hk-bacterial strains (10^8 CFU) induced acute pain responses similar to the relative efficacies of nociceptor activation *in vitro* (Fig. 3d). Hk-*S. aureus* and hk-*S. pneumonia*, which caused the most acute pain following injection, also induced mechanical and heat hyperalgesia (Supplemental Fig. 12).

What heat-stable molecular elements within bacteria mediate nociceptor activation? Application of *S. aureus* peptidoglycans and lipoteichoic acid (LTA) did not produce calcium flux in DRG neurons (Supplemental Fig. 13), and together with *in vivo* data (Fig. 2), suggests that TLR2 ligands do not contribute significantly to *S. aureus* pain. We therefore investigated the contribution of other bacterial molecules. N-formylated peptides, found in bacteria and mitochondria, are recognized by G-protein coupled formyl peptide receptors (Fprs) on leukocytes to mediate immune chemotaxis during infection[21]. Mouse vomeronasal neurons express Fprs, so may detect formyl peptides during olfaction[22,23]. We found that fMLF, an *E. coli* derived peptide, and fMIFL, a *S. aureus* derived peptide[24], induced calcium flux in a subset of DRG neurons that also responded to capsaicin and to allyl isothiocyanate (AITC), a TRPA1 ligand (Fig. 3e, Supplemental Fig. 14). Moreover, unformylated MIFL activated fewer DRG neurons than fMIFL (Fig. 3e), similar to formyl group requirements for immune cell activation. When injected, fMLF and fMIFL induced mechanical but not heat hyperalgesia (Fig. 3f). This selective mechanical pain induction may be related to the restricted activation by formyl peptides of AITC-responsive neurons (Supplemental Fig. 14), which are mainly C-mechanosensitive fibers[25]. DRG and trigeminal ganglia express Fpr1 and Fpr2 (Fpr-rs2), but not other Fprs (Supplemental Fig. 15). Microarray analysis of purified Nav1.8-cre/TdTomato^{+} nociceptors confirmed the specific expression of Fpr1, but not Fpr-rs1, 3, 4, or 7 (Supplemental Fig. 16). These data indicate that nociceptor activation may be mediated through Fpr1, which recognize fMLF and fMIFL in immune cells[24]. The Fpr1 antagonist Boc-MLF reduced neuron activation by fMLF and hk-bacteria (Supplemental Fig. 17). Fpr1$^{-/-}$ mouse DRG neurons showed decreased fMIFL calcium flux, and Fpr1$^{-/-}$ mice showed reduced mechanical hyperalgesia following fMIFL injection relative to WT mice (Supplemental Fig. 17). While live *S. aureus* pain peaks at 6 hours, time-courses may differ for hk-bacteria and ligands, which are influenced by ligand diffusion and clearance kinetics. Ruthenium Red significantly decreased fMIFL responses in amplitude and proportion, indicating that formyl peptides may gate a downstream large pore calcium ion channel (Supplemental Fig. 18). Heat-treatment did not affect fMIFL molecular composition or the ability of fMIFL to induce hyperalgesia following injection (Supplemental Fig. 19). Importantly, Fpr1$^{-/-}$ mice showed reduction in mechanical but not heat hypersensitivity following injection of hk-*S. aureus* (Fig. 3g). Thus, formyl peptides are heat-stable elements within bacteria that contribute to activation of mechanical hypersensitivity.

Live bacteria actively release formyl peptides[26] and secrete a host of virulence factors including pore-forming toxins (PFTs) to facilitate tissue dissemination[6,7,8,27,28,29]. We found that *S. aureus* culture supernatant induced calcium flux in DRG neurons (Supplemental Fig 20). Alpha-hemolysin (Hla) is a PFT secreted by nearly all *S. aureus* strains, playing a role in tissue damage, bacterial spread, and inflammation[27,28,29]. When flowed onto DRG neurons, Hla induced immediate calcium flux in nociceptors, which could be washed out by buffer (Supplemental Fig. 20). Hla inserts into cell membranes and assembles into heptameric pores that allow non-selective entry of cations[29], which may be sufficient to depolarize neurons. We found that prolonged bath application of Hla on DRG neurons elicited sustained bursts of calcium flux (Fig. 4a), selectively in capsaicin-responsive neurons (Supplemental Fig. 21). Hla induced a dose-dependent calcium flux in DRG neurons (EC_{50} 356 nM, Fig. 4b). Hla binds to cells via A Disintegrin and Metalloprotease 10 (ADAM10), leading to membrane pore assembly[27,30]. ADAM10 expression was detected by RT-PCR in DRG and trigeminal ganglia (Supplemental Fig.15). Using an antibody that recognizes the ADAM10 ectodomain, we found that a subset of Nav1.8-Cre/TdTomato^{+} nociceptors (59.8%) expressed surface ADAM10 but not TdTomato^{-} cells, which may contribute to selective nociceptor activation (Supplemental Fig.22). *In vivo*, Hla injection induced significant acute pain behavior in a dose-dependent manner (EC_{50}=6.3 pmoles, Fig. 4c). Heat pre-treatment abolished the ability of Hla to

induce pain (Fig. 4d), indicating that this mechanism of nociceptor activation is separate from heat-stable elements (Fig. 3). Hla also evoked action potential firing in DRG neurons (Fig. 4e). Hla neuronal activation did not involve voltage-gated calcium channels or large-pore cation channels (not blocked by $CdCl_2$ or Ruthenium Red, absent in TRPV1$^{-/-}$) but did require external calcium (Supplemental Fig. 23). Therefore, Hla nociceptor activation appears to be independent of most endogenous calcium ion channels, and its ability to assemble into membrane-perforating pores may be sufficient for neuronal depolarization. H35L mutant Hla (Hla_{H35L}), which cannot form a stable oligomer or pore, did not evoke action potentials (Fig. 4e) or calcium flux in DRG neurons (Supplemental Fig. 23). Hla_{H35L}, unlike WT Hla, did not produce acute pain in mice (Fig. 4f). Hla was sufficient to induce mechanical, heat, and cold hypersensitivity (Fig. 4g). Finally, we found that an isogenic *S. aureus* mutant devoid of Hla expression caused significantly less hyperalgesia than WT bacteria (Fig. 4h). Therefore, we conclude that Hla contributes to pain during *S. aureus* infection in a manner dependent on pore-formation.

Nociceptor neuropeptides regulate inflammation

Nociceptor activation results in release of neuropeptides from peripheral terminals which can induce vasodilation and neurogenic inflammation[31]. To understand the role of nociceptors in modulating the immune response, we generated Nav1.8-Cre/Diphtheria Toxin A (DTA) mice to specifically ablate these cells[32]. Nav1.8-Cre/DTA DRG neurons did not show calcium flux upon hk-bacteria stimulation (Fig. 5a). Mechanical and thermal hypersensitivity following *S. aureus* infection was abolished in Nav1.8-Cre/DTA mice, indicating that Nav1.8-lineage neurons are the major cell-type mediating bacterial pain (Fig. 5b). Granulocytes were found 24 hours post-infection near Nav1.8-Cre/TdTomato$^+$ nerve fibers (Supplemental Fig. 24), and when co-cultured, DRG neurons also formed close contacts with neutrophils and macrophages (Supplemental Fig. 25), raising the question of whether nociceptors may act on immune cells. Following infection, Nav1.8-Cre/DTA mice displayed significantly increased tissue swelling relative to control littermates (Fig. 5c). Bacterial load did not differ significantly between the mice (Supplemental Fig. 26). Nav1.8-Cre/DTA mice showed increased infiltration of neutrophils/monocytes at infection sites (Fig. 5d). The popliteal lymph node which drains the footpad[33], was significantly larger in Nav1.8-Cre/DTA mice following *S. aureus* infection by weight and cellularity (Fig. 5e, Supplemental Fig. 27). There was a difference in baseline lymph node size, but the increase was substantially greater in Nav1.8-Cre/DTA than control mice post-infection. Nav1.8-Cre/DTA tissues also showed increased TNF-α (Supplemental Fig. 28), a cytokine that drives lymphadenopathy (hypertrophy) of the draining lymph node during bacterial infection[45]. This lymphadenopathy was localized, as downstream inguinal lymph nodes and spleens were not enlarged in infected Nav1.8-Cre/DTA mice (Supplemental Fig. 27). The popliteal lymphadenopathy was due to increased T cells, B cells, and monocytes (Fig. 5e). Thus, nociceptor ablation led to increased local inflammation. To determine molecular factors that mediate this immunomodulation, we performed microarray analysis of flow cytometry purified Nav1.8-Cre/TdTomato$^+$ nociceptors from dorsal root, trigeminal, and nodose ganglia (Fig. 6a). Neuropeptide expression levels were ranked based on a neuropeptide database (www.neuropeptides.nl; Fig. 6b, full dataset in Supplemental Fig. 29). Microarray data from innate immune cell subsets[34] were analyzed for neuropeptide receptor levels. CGRP, Galanin (Gal), Somatostatin (Sst) receptors showed the highest expression in neutrophils, monocytes, macrophages; these neuropeptides were also highly expressed in purified nociceptors (Fig. 6b, full dataset in Supplemental Fig. 30). *In vitro*, we found that CGRP, Gal, and Sst all suppressed TNF-α release from macrophages stimulated with hk-*S. aureus* or LTA (Fig. 6c, complete analysis in Supplemental Fig. 31). Furthermore, *S. aureus* supernatant and Hla induced CGRP release from DRG neurons in dose-dependent manner (Fig. 6d). CGRP injection during *S. aureus* infection did not alter inflammation at the

infection site, but significantly suppressed lymphadenopathy of the draining lymph nodes (Fig. 6e, Supplemental Fig. 32). Therefore, upon infection, nociceptors may release neuropeptides that directly modulate innate immune activation.

Discussion

We analyzed mechanisms responsible for nociceptor activation during *S. aureus* infection, which commonly causes pain. We found that bacterial-derived factors directly activated nociceptors and contributed to hyperalgesia *in vivo*. N-formylated peptides and the PFT Hla induced direct neuronal responses through distinct mechanisms: formyl peptides through Fpr1 and Hla through pore-assembly leading to ionic influx (diagram, Supplemental Fig. 33).

Direct activation of nociceptors by bacteria is likely a major mechanism leading to pain, especially early in *S. aureus* infection during active pathogen expansion (Fig. 1, 3-4). Following immune cell infiltration, bacteria are largely eliminated, concurrent with TNF-α production, and although pain is reduced it remains (Fig. 1). Immune-mediated mechanisms may play a role at these later time-points. Live infection is complex and our blockade of host defenses may also enhance direct pathogen mediated mechanisms.

Pathogen virulence and immunogenicity likely contribute to the degree of direct nociceptor activation. USA300/LAC is a highly virulent strain, expressing several PFTs in addition to Hla including β, γ-hemolysins, PVL, and Phenol soluble modulins[7,8,9]. *S. aureus* also possesses effective immune evasion mechanisms, including toxins that lyse immune cells, Staphylococcal Protein A which impairs antibody function, and complement evasion strategies[8, 35]. Thus additional elements from the bacterial proteome likely exist that may activate nociceptors. *E. coli* and other Gram-negative bacteria also induce painful infections, and lipopolysaccharides have been found to sensitize TRPV1[15]. The balance of nociceptor activation by pathogenic and immune mechanisms may differ between dissimilar pathogenic bacteria species.

Although peripheral nociceptor activation contributes to neurogenic inflammation, inducing vasodilation and capillary permeability[31], we found that ablation led to increased immune influx and lymphadenopathy, implying pain-mediated immune-suppression. Our data support a role for neuropeptides in regulating innate immune activation that occurs later than the acute vascular phase of inflammation. Receptors for CGRP, Gal, Sst are expressed by myeloid immune subsets, and these neuropeptides have been shown to have inhibitory functions on immunity[36,37,38]. In particular, CGRP dampens TNF-α transcription in dendritic cells through a cAMP-dependent repressor mechanism[36,39]. CGRP down-regulates cytokine levels in endotoxic shock[40], and conversely, $TRPV1^{-/-}$ mice display increased inflammation during sepsis[41].

Potent immunomodulatory neural reflex circuits also exist that maintain immune homeostasis[42]. In *C. elegans*, a sensory neural circuit suppresses innate immunity and modulates survival during bacterial infection[43]. In mammals, vagal efferents suppress splenic macrophage activity, protecting against bacterial endotoxic shock[42,44], and activation of liver autonomic fibers modulates NK T-cell activity, leading to increased bacterial infection[45]. It has been hypothesized that sensory neurons initiate mammalian neural circuits[42], but a direct immunosuppresive role of nociceptive fibers, as revealed here, was not suspected. Lymph node swelling during infection is often accompanied by pain, and nociceptor activation may limit immune influx into lymph nodes. Both nociceptive and autonomic fibers innervate lymph nodes[46]; therefore, lymph node suppression may act through local neuropeptide release or initiation of autonomic reflex circuits. Highly

pathogenic bacterial strains may have evolved the ability to exploit these neural-mediated immune regulation pathways for virulence and spread within infected tissues, by producing more nociceptor activation and greater immunosuppression.

In conclusion, our data reveal an unsuspected mechanism for pain induction during bacterial infection, a direct pathogen-mediated activation of nociceptors. This neuron-pathogen interaction leads to a down regulation of the local inflammatory response. The nervous system plays therefore, direct sensory and modulatory roles in host-pathogen interactions during acute *staphylococcal* infection.

Full Methods

Mice

C57BL/6, B6.TLR2$^{-/-}$, B6.MyD88$^{-/-}$, B6.RAG1$^{-/-}$, B6.TdTomato reporter mice (ai14 line[47], B6.Zsgreen mice, B6.DTA reporter mice[48], B6.TRPV1$^{-/-}$ mice, Nod.scid.gamma, Nod.WT mice purchased from Jackson Laboratories (ME, USA); B6.Fpr1$^{-/-}$, B6.WT controls purchased from Taconic Farms (NY, USA). Nav1.8-Cre (SNS-Cre) mice[20] were a gift from Rohini Kuner (University of Heidelberg, Germany). Nav1.8-Cre mice were bred with B6.TdTomato, B6.Zsgreen mice to generate Nav1.8-Cre/TdTomato and Nav1.8-Cre/Zsgreen mice. Nav1.8-Cre$^{+/-}$ mice were bred with B6.DTA$^{+/+}$ mice to generate nociceptor deficient Nav1.8-Cre$^{+/-}$/DTA$^{+/-}$ and control littermates (Nav1.8-Cre$^{-/-}$/DTA$^{+/-}$). For infection and behavioral experiments, adult, 7-14 week male mice were used, except for when age-matched, male and female Nav1.8-Cre/DTA with control littermates were used. All bacterial and animal experiments were conducted according to institutional animal care and safety guidelines at Boston Children's Hospital and Harvard Medical School.

Statistical analysis

Sample sizes for all experiments were chosen according to standard practice in the field. Bar and line graphs are plotted as mean±standard error (s.e.m.), and in some cases, individual mice are plotted as dots. "n" represents the number of mice used in each group. Statistical analysis of behavioral data of mechanical, heat, and cold, as well as tissue swelling time-courses was conducted by Two-way repeated measures (RM) ANOVA, with Bonferroni post-tests conducted for each time-point tested. In these behavioral analyses, saline injected mice or wild-type mice served as control groups for each statistical comparison.

For electrophysiology, significance was calculated using the Mann-Whitney test. Statistical comparisons of acute nocifensive behavior (total time licking/biting in 20 minutes), tissue bacterial load, tissue swelling measurements, immune cell influx, neuronal responses by calcium imaging, CGRP and TNF-α levels were by unpaired, student's t-test. In acute pain analysis, saline injected mice were compared to treatment groups. In CGRP and TNF analysis, buffer treated cells were controls for comparisons. In calcium imaging, proportion of neuronal responses from at least 3 fields were quantified. Data was plotted using Prism (Graphpad, CA, USA).

Behavioral analysis

All animals were acclimatized to the behavioral testing apparatus used on at least three habituation sessions. At least two baseline measures were obtained for each behavioral tests prior to testing. To measure mechanical sensitivity, animals were placed on an elevated wire grid and the lateral plantar surface of the hindpaw stimulated with von Frey monofilaments (0.007–8 g). The withdrawal threshold was determined as the filament at which the animal withdrew its paw at least five in ten applications. To measure cold sensitivity, animals were placed on an elevated wire grid, a drop of acetone applied to the plantar hindpaw by syringe.

The duration of time that animal elevated or licked the paw over a 90 s period immediately after acetone application was measured. To measure heat sensitivity, mice were plated on the glass plate of a Hargreave's apparatus set at 29°C (IITC Life Science, CA, USA), and a radiant heat source applied to the plantar hindpaw. Latency to hindpaw flicking/licking was recorded (maximum of 30 s). Acute nocifensive behavior was scored by observation of mice under a glass beaker following intraplantar injection. Time spent lifting/flinching/licking the hind-paw was recorded in 5-minute intervals. Acute nocifensive behavior was quantified as the total licking/lifting in the first 20 minutes post-injection. In infection and compound injection experiments, observers were blinded to mouse genotype/strain. When different substances were compared within experiments, animals were randomized so similar group mean baseline thresholds were present.

Bacterial strains

S. aureus CA-MRSA strains LAC/USA300 and LAC/300 deficient in Hla were generated as described previously[6,27]. Strains were grown in tryptic soy broth (TSB) and tryptic soy agar (TSA) (BD Biosciences, CA, USA). GFP-LAC/USA300 strain AH1726 was generated by transforming GFP-expressing, chloramphenicol-resistant plasmid pCM29[50] into LAC. Plasmid DNA was electroporated into *S. aureus* as previously described[51]. The resulting strain produces GFP in a constitutive manner from the *sarA* P1 promoter, and maintained in TSB or TSA supplemented with 10 μg/mL chloramphenicol.

S. aureus infection model and tissue measurements

S. aureus strains were grown overnight in TSB to log phase, pelleted, and resuspended in 0.9% saline at different dilutions. OD_{650} was measured to estimate bacterial density, with confirmation by TSA plating. For infection, 20 μL of bacteria (5×10^6 CFU) in 0.9% saline was injected subcutaneously into the hindpaw plantar surface using a 25 μL syringe fitted with a 26-gauge needle (Hamilton Co, NV, USA). Mice were monitored closely following injection, and assayed for pain behavior at different intervals. For neutrophil/monocyte depletion, mice were injected intra-peritoneally (i.p.) with GR1 antibody (clone RB6-8C5, Bio-XCell, NH, USA) at a dose of 400 μg/200 μL PBS, 24 hours and one hour prior to bacterial injections. Control rat IgG (Jackson Immunoresearch, ME, USA) was injected at the same dosage. For neuropeptide experiments, CGRP, Galanin, somatostatin (Tocris, MN, USA, doses of 1 pmol/200 μL saline) were injected i.p. into mice at 24 hours, 4 hours prior to infection, and 4 hours, 20 hours post-infection. As controls, saline was injected at the same time-points. For tissue swelling analysis, a digital micrometer (Mitutoyo, MA, USA) was used to measure thickness of the plantar area prior to and at defined time-points post-infection. Thickness increase was calculated as differences from baseline measurements (or as % increase normalized to baseline). For bacterial load determination, total paw tissue from epidermis to the tendons was dissected onto ice and weighed, dissociated by dounce homogenizer (Wheaton, NJ, USA) in 1 mL PBS, serial dilutions made, plated on TSA plates, and bacterial recovery determined by counting colonies after overnight incubation (normalized by dissected tissue weight). GFP-LAC strain was grown on TSA plates with 10 μg/mL chloramphenicol.

Neuronal cultures and calcium imaging

Dorsal root ganglia (DRG) from adult mice (7-12 weeks) were dissected into Neurobasal-A medium (Life Technologies, CA, USA), dissociated in 1 mg/mL Collagenase A+2.4 U/mL dispase II (enzymes, Roche Applied Sciences, IN, USA) in HEPES buffered saline (Sigma, MO, USA) for 70 minutes at 37°C. After trituration with glass pasteur pipettes of decreasing size, DRG cells were centrifuged over a 10% BSA gradient, plated on laminin-coated cell culture dishes in B27 supplemented Neurobasal-A medium+50 ng/mL Nerve Growth Factor (NGF)+Penicillin/Streptomycin (Life Technologies). For bacterial co-cultures, Nav1.8-Cre/

TdTomato or Nav1.8-Cre/ZsGreen DRG neurons were plated in poly-lysine, laminin pre-coated, 8-well chamber slides (Lab-Tek) overnight at 37°C. 10^6 CFU GFP-*S. aureus* or CMTMR labeled *S. pneumoniae* were added in Neurobasal-A to DRG neurons for 2 hours at 37°C; co-cultures were fixed with 4% PFA, mounted in Vectashield (Vector Labs, CA, USA) for microscopy. DRG neurons were used for calcium imaging and electrophysiology 16-48 hours post-plating.

For calcium imaging, cells were loaded with 10 μM Fura-2-AM (Life Technologies) at 37°C for 45 min in Neurobasal-A medium, washed into Standard Extracellular Solution (SES, 145 mM NaCl, 5 mM KCl, 2 mM $CaCl_2$, 1 mM $MgCl_2$, 10 mM glucose, 10 mM HEPES, pH 7.5), and imaged at room temperature. Cells were illuminated by an UV light source (Xenon lamp, 75 watt, Nikon, NY, USA), 340 nm and 380 nm excitation alternated by a LEP MAC 5000 filter wheel (Spectra services, NY, USA), and fluorescence emission captured by Cool SNAP ES camera (Princeton Instruments, NJ, USA). 340/380 ratiometric images were processed, background corrected, and analyzed with IPLab software (Scientific Analytics, CA, USA). Microsoft Excel was used for further analyses (Microsoft, USA). Ligands were flowed directly onto neurons using perfusion barrels followed by buffer washout and further application, or applied to the culture bath at the beginning of imaging. In some experiments, 1 μM capsaicin (Tocris), 100 μM AITC (Sigma) or 40 mM KCl (Sigma) was applied following bacterial ligands.

Electrophysiology

Whole-cell transmembrane voltages of DRG neurons were recorded at room temperature (21±1°C) in the current-clamp mode using an Axopatch 200A amplifier (Molecular Devices, CA, USA). The internal pipette solution consisted of (mM): 140 KCl, 5 NaCl, 2 $MgCl_2$, 0.5 $CaCl_2$, 5 EGTA, 10 HEPES, 3 Na_2ATP, and 0.1 MgGTP (pH 7.4 with KOH). The extracellular solution consisted of the following: 145 NaCl, 5 KCl, 2 $CaCl_2$, 1 $MgCl_2$, 10 HEPES, and 10 glucose (pH 7.4 with NaOH). Data were sampled at 5–10 kHz and analyzed using pCLAMP 10.2 (Molecular Devices). Resting membrane potentials of DRG neurons were typically −60 to −65 mV and cell body diameters were 15 to 25 μm.

For multi-electrode arrays, DRG neurons were isolated as described, plated on MED-P515A 64-electrode probes, and recorded using a MED64 device (Alpha Med Scientific, Osaka, Japan). Recombinant Hla was applied at 30 μg/mL concentration. Spikes were identified using Mobius software (Alpha Med Scientific, Osaka, Japan), and histogram analysis was performed in Matlab (Mathworks, MA, USA).

Bacterial ligands

For heat-killed bacteria experiments, to standardize titers used for differential comparisons, we used bacteria purchased from Invivogen (CA, USA; 10^{10} CFU, each heat-treated for 30 min at 120°C.): hk-*S. aureus*, American-type tissue culture (ATCC, VA) strain 6539 Rosenbach; hk-*S. pneumoniae*, NETC7466; hk-*H. pylori*, ATCC strain 43504, NTCTC 11637; hk-*L. monocytogenes*, strain 9668P; hk-*M. fermentans*, ATCC strain 19989; hk-*P. aeruginosa*, strain ATCC strain BAA-47. For calcium imaging, bacteria were dissolved in SES at 10^7 CFU/mL. We note that bacterial addition did not affect pH, which remained at pH7.5. For injections, hk-bacteria strains were dissolved in 0.9% saline, 20 μL hk-bacteria (10^8 CFU total) was injected into the hind paw using a Hamilton syringe fitted with a 26-gauge needle.

N-formal peptides were synthesized by Foci solid-phase peptide synthesis and the peptides were formylated by 2,2,2-trifluoroethyl formate[52]. HLPC resulted in the pure compounds: fMLF, fMIFL, and MIFL, which were confirmed by MS and NMR. Peptides were stored at

10 mM concentration dissolved in DMSO (Thermo Fisher, MA, USA) at −20°C. For calcium imaging, fMLF, fMIFL, MIFL were dissolved in SES to 1 μM concentration. For intraplantar injections, fMLF and fMIFL were dissolved in 0.9% saline, and 1.0 μg of fMLF (2.1 nmoles) or 1.3 μg of fMIFL (2.04 nmoles) injected in a 20 μL volume.

For *S. aureus* supernatant collection, LAC bacteria were cultured overnight in TSB, removed by centrifugation, and resulting supernatant diluted to 5% in SES buffer for application to DRG neurons. Recombinant *S. aureus* Hla and mutant H35L (Hla_{H35L}) were generated and purified as previously described[30]. Commercial Hla (Sigma) induced comparable results *in vitro* and *in vivo*. In some imaging experiments, Hla was bath applied or flowed directly onto neurons at 10 μg/mL (Fig. 4A, Supplemental Fig. 20). For pain behavioral studies, Hla and Hla_{H35L} dissolved in 0.9% saline was injected in 20 μL volume into the hind-paw at described doses. For heat-inactivation, the same batch of fMIFL or recombinant Hla was split into two aliquots, one of which was treated at 100°C for 30 minutes. Untreated or heat-treated substances were used for mass spectrometry and pain hypersensitivity studies.

Whole well imaging of calcium flux

DRG neurons were seeded in B27 supplemented Neurobasal-A at 2000 neurons/well in laminin coated 384 well microplates (Greiner, NC, USA) at 37°C for 24 hours. Neurons were loaded with Fura-2 AM for 30 minutes at 37°C, then washed twice with HBSS (Life Technologies). A Hamamatsu FDSS 7000EX kinetic reader was used to dispense ligands onto DRG neurons and calcium flux recorded every 1.9 seconds at room temperature for 30 minutes total. To evaluate the role of extracellular cations, cells were analyzed in calcium/magnesium-free HBSS (Life Technologies). For related experiments, EDTA (5 mM) or HBSS was added to wells during recording to evaluate Hla flux.

Immune stimulation and neuro-immune co-cultures

For peritoneal macrophages, 0.5 mL Brewer's thioglycollate solution (2%) was injected i.p. into mice; 4 days later, animals were euthanized and peritoneal cavities flushed using 10 mL DMEM/10% Fetal calf serum (FCS). Cells were plated in 96-well plates at 5,000 cells/well. For bone marrow derived macrophages, tibias, femurs of C57BL/6 mice were flushed using 27 gauge needle, and bone marrow plated in 15 cm petri dishes in DMEM/10%FCS/50μMβ-mercaptoethanol (β-me)/20%L929 conditioned media for 7 days. Differentiated macrophages were dislodged from plates using non-enzymatic dissociation media in HBSS (Sigma), and plated into 96-well plates at 5,000 cells/well in DMEM/10%FCS/50μM β-me. α-CGRP (rat), Somatostatin, Galanin (Tocris) were used at different concentrations in macrophage stimulation assays. Peritoneal macrophages were stimulated with 10^7 CFU/mL hk-*S. aureus* (Invivogen) and bone marrow macrophages stimulated with 1 μg/mL *S. aureus* derived LTA (Invivogen) for 16 hours in DMEM/10%FCS; TNF-α levels in culture supernatant were determined using an ELISA kit (Biolegend).

For neuron-macrophage co-cultures, DRG neurons were isolated and bone marrow macrophages derived as described above, resuspended together in Neurobasal-A/2%FCS/50 ng/mL NGF, and co-plated at a density of 2000 neurons+10,000 macrophages/well into laminin/poly-D-lysine coated 8-well chamber slides (Lab-Tek); co-cultures were fixed with 4% PFA after 20 hours. For neuron-neutrophil co-cultures, DRG neurons were cultured overnight in 8-well chamber slides at 2000 cells/well. Neutrophils were isolated as described[53,54]: briefly, bone marrow from tibias, femurs was depleted of red blood cells with ACK (0.15 M NH4Cl, 10 mM KHCO3, 0.1 mM EDTA), run over a discontinuous 52%, 69%, 78% percoll gradient for 30 minutes at 1500 g. The 69%/78% interface and 78% layer containing neutrophils were harvested, washed, resuspended in neurobasal medium/2% FCS/50 ng/mL NGF and added at 10000 cells/well to DRG neurons; co-cultures were

washed and fixed with 4% PFA after 6 hours. Immunostaining was performed with anti-βIIITubulin (Tuj1, 1:1000), rat anti-CD11b (Biolegend, 1:100), followed by Alexa 568 goat anti-mouse IgG (Life Technologies, 1:500) or Alexa 488 goat anti-rat IgG (Life Technologies, 1:500), and imaged by epifluorescence microscopy.

RT-PCR and quantitative PCR

RNA was extracted from mouse bone marrow, spleen, kidneys, whole DRG, trigeminal ganglia, or 24 hours. DRG neuron cultures using Qiazol reagent, followed by the RNeasy mini kit (Qiagen, MD). DNase I treatment (Qiagen) was used to remove genomic DNA, cDNA reverse transcribed using Superscript III with random hexamers (Life Technologies). PCR was conducted for 32 cycles on a Mastercycler Pro thermocycler (Eppendorf, Hamburg, Germany), products run on agarose gels. RT-PCR primers were synthesized by integrated DNA technologies (IA, USA). Primer sequences: ADAM10, Forward – 5'ATGGAGCAAACATGGCATAA3'; Reverse – 5'GCAACATCTGGGGACAAACT3'. β-actin, Forward - 5'TGTTACCAACTGGGACGACA3'; Reverse - 5'TCTCAGCTGTGGTGGTGAAG3'. Fpr1, Forward – 5'CAGCCTGTACTTTCGACTTCTCC3'; Reverse – 5'ATTGGTGCCTGTATCACTGGTCT3'. Fpr-rs1, Forward – 5'GGCAACTCTGTTGAGGAAAG3'; Reverse – 5'AATGAACTGGTTGGATTAAC3'. Fpr-rs2), Forward-5'CTTTATCTGCTGGTTTCCCTTTC3'; Reverse – 5'CTGCTGCTTGAATCACTGGTTTG3'. Fpr-rs3, Forward-5'TGACACCTTTAATTGCTCCT3'; Reverse-5'GTTTCTTAATCACTCTCATTGC3'. Fpr-rs4, Forward-5'CAAGAGGGGATGTGTACTGT3'; Reverse-5'TGTTAAAGGAAGCCAAGGTA3'. Fpr-rs6, Forward-5'CCCCTGAGGAGCAAGTAAAAGTAT3'; Reverse-5'CAGGGCTGAGTCCTCCCTTA3'. Fpr-rs7, Forward-5'CCTGAGGAGCAGGTAAACATGT3'; Reverse-5'GGGCTGAATCCTCCCTCA3'.

For qPCR, cDNA was subjected to 2-step thermocycling using fast SYBR green master mix (Life Technologies), data collection performed on an Applied Biosystems 7500 machine (Life Technologies). The following primers were used: Fpr1, Forward – 5'CATTTGGTTGGTTCATGTGCAA3'; Reverse – 5'AATACAGCGGTCCAGTGCAAT3'. Fpr-rs2 (FPR2) was based on Liberles et al[22], Forward -5'TGACTACTGTTAGAATTCCTG3'; Reverse-5'GATAGCTGTGTTCAACTTTTCTTCAT3'. Gapdh, Forward – 5'TGGCAAAGTGGAGATTGTTGCC3'; Reverse – 5'AAGATGGTGATGGGCTTCCCG3'. Expression levels were normalized to Gapdh using the ΔΔcT method.

Flow cytometry analysis of infected tissues and lymph nodes

Paw tissue was minced and digested in 1 mg/mL Collagenase A/2.4 U/mL Dispase II (Roche Applied Sciences) in HEPES buffered saline (Sigma) for 2 hours at 37°C. Following digestion, cells were washed into HBSS (Life Technologies) with 0.5% Bovine serum albumin (BSA, Sigma), filtered through a 70 micron mesh, resuspended in HBSS/0.5% BSA, blocked with FcBlock (rat anti-CD16/CD32; 1:10 hybridoma supernatant) on ice for 5 min, and incubated with mixtures of the following antibodies: anti-CD11b-PE (Biolegend, CA, USA, 1:1000), anti-CD45-PercP (Biolegend, 1:200), anti-Ly-6G-APC (Biolegend, 1:200), anti-Ly-6C-FITC (Biolegend, 1:200). Flow cytometry was conducted on a FACSCalibur machine (Bectin Dickinson) equipped with an argon and helium-neon laser.

Lymph nodes were dissected into 5 mL RPMI-1640 on ice. After dissections, RPMI-1640 was removed and replaced with 2 ml enzyme mix: RPMI-1640 containing 0.8 mg/ml Dispase+0.2 mg/ml Collagenase P (both from Roche)+0.1 mg/ml DNase I (Life Technologies). Tubes were incubated at 37°C in a waterbath and inverted at 5 min intervals to ensure well-mixing. After 20 min, lymph nodes were gently aspirated and expirated using a 1-ml pipette, which disrupts the capsule to release leukocytes. The mixture was replaced in the waterbath and large fragments allowed to settle for 30 s, after which the enzyme mix was removed and added to 10 ml of ice-cold FACS buffer (0.5% BSA, 2 mM EDTA, 10mM NaN3, 15mM HEPES in PBS, pH7.4). 2 mL of fresh enzyme mix was added to the digestion and the process was repeated until all lymph node fragments were completely digested. Cells were filtered through 80 μm nylon mesh and counted by hemocytometer. 5×10^6 cells were incubated with 50 μl diluted antibodies (TCRβ, CD11b, Ly6C, Ly6G, CD19, antibodies from Biolegend) for 20 min at 4°C in FACS buffer before acquisition on a FACSCalibur or FACSAria II (BD Biosciences). Neutrophils were considered $CD11b^+Ly6G^+$, monocytes $CD11b^+Ly6G^-Ly6C^+$, B cells CD19+, T cells TCRβ+. Flow cytometry data was analyzed using FlowJo software (TreeStar, OR, USA).

Immunostaining and microscopy

Mice were transcardially perfused with PBS followed by 4% PFA/PBS (Sigma). Plantar tissue was dissected, post-fixed for 2 hours, cryoprotected in 30% sucrose/PBS, embedded, and frozen in Optimal cutting temperature compound (OCT, Electron Microscopy Sciences, PA). Tissues were stored at −80°C until sectioning. Cryosections were cut at 50 μm thickness onto Superfrost plus slides (Thermo Fisher). For hematoxilin and eosin, sections were dehydrated by sequential alcohol steps, mounted in Permount medium (Thermo Fisher), and imaged by light microscopy on a BZ-II analyzer at 15X magnification (Keyence, Osaka, Japan). For immunostaining, sections were stained with GR1-Alexa 647 antibody (Biolegend, 1:100) for 2 hours at room temperature, mounted in Vectashield with DAPI (Vector Labs) and imaged using an LSM700 laser-scanning confocal microscope (Carl Zeiss, Germany). 10X Zeiss EC plan-NEOFLUAR dry and 63X Zeiss plan-APOCHROMAT oil objectives were used, with z-stacks of 40 μm total imaged at 1 μm steps; maximum projection images were exported for presentation.

For DRG, tissues were dissected, post-fixed, embedded in OCT as described above. 14 μm cryosections were cut and stained with rabbit anti-CGRP (Millipore, MA, PC205L, 1:500) followed by Alexa 488-anti-rabbit IgG (Life Technologies, 1:1000) or chicken anti-neurofilament (Millipore, AB5539, 1:500), followed by Alexa 488 anti-chicken IgG (Life Technologies, 1:1000). Sections were mounted in Vectashield with DAPI (Vector Labs), and imaged by Eclipse 50i epifluorescence microscope (Nikon, NY, USA).

Flow cytometric purification of nociceptors and ADAM10 staining

DRG, trigeminal, or nodose ganglia from Nav1.8-Cre/TdTomato mice were dissected, dissociated into single cells by enzymatic digestion (1 mg/mL Collagenase A+2.4 U/mL dispase II (Roche Applied Sciences) in HEPES buffered saline (Sigma)) for 60 minutes at 37°C, filtered through a 70 micron filter, and stained with DAPI (Sigma, 20 ng/mL) as a dead cell stain in HBSS/0.5% BSA. Nociceptors were sorted on a FACSaria II machine (Bectin Dickinson) using a yellow-green laser to detect TdTomato fluorescence (Gates, Fig. 6, Supplemental Fig. 14). To determine purity, cells were sorted into Neurobasal-A and plated onto laminin coated glass slides for microscopy. For microarrays, neurons were sorted directly into Qiazol reagent (Qiagen). For ADAM10 surface staining, Nav1.8-Cre/TdTomato DRG were dissociated and stained with rat anti-ADAM10 ectodomain antibody (clone 139712, R&D systems; reviewed, 1DegreeBio) or with rat IgG2A isotype control (clone RTK2758, Leaf purified, Biolegend) for 1 hour on ice (5 μg/mL each). After washing

with HBSS, cells were incubated with Alexa 488 goat anti-rat IgG (4 μg/mL, Life technologies) for 30 minutes on ice. Following two washes with HBSS, cells were resuspended in HBSS/0.5% BSA and analyzed on a BD FACSaria II machine. Flow cytometry data was analyzed using FlowJo (Treestar).

Microarray analysis

Total RNA was extracted by sequential Qiazol extraction and purification through RNeasy micro kit with on column genomic DNA digestion (Qiagen). RNA quality was determined by Agilent 2100 Bioanalyzer using the RNA Pico Chip (Agilent). RNA was amplified into cDNA using the Ambion WT expression kit for Whole Transcript Expression Arrays, with Poly-A controls from the Affymetrix Genechip Eukaryotic Poly-A RNA control kit. The Affymetrix Genechip WT Terminal labeling kit was used for fragmentation, biotin labeling. Affymetrix GeneChip Hybridization control kit and the Affymetrix GeneChip Hybridization, wash, stain kit was used to hybridize samples to Affymetrix Mouse Gene ST 1.0 GeneChips, fluidics performed on the Affymetrix Genechip Fluidics Station 450, and scanned using Affymetrix Genechip Scanner 7G (Affymetrix). Microarray work was conducted at the Boston Children's Hospital IDDRC Molecular Genetics Core, which is supported by NIH-P30-HD 18655. Affymetrix CEL files were normalized with the Robust Multi-array Average (RMA) algorithm with quantile normalization, background correction, and median scaling. The ImmGen dataset was also analyzed (GEO no. GSE15907). Heat-maps were generated using GenePattern platform (Broad institute, MIT). Nociceptor microarray datasets are deposited at the GEO database under accession no. GSE46546.

Supplementary Material

Refer to Web version on PubMed Central for supplementary material.

Acknowledgments

We thank Lee Barrett, Victor Wang, Nick Andrews, Cassidy Melin, Yixiao Wang, Kelly Duong, Enrique Cobos del Moral, Olesegun Babanyi, Gregory Bryman for technical help. We thank Yung-Chih Cheng, Russell Becker for technical advice; Jared Sprague, Ajay Yekkirala for developing whole-well imaging; Ichiro Inoshima for recombinant Hla; Rick Malley, Judith Steen, Qiufu Ma for helpful discussions; Joshua, Tammy Chiu for moral support; Steve Liberles, Bing Xu, Vijay Kuchroo for mentoring. This work was supported by NIH PO1AI078897, 5RO1AI039246 (MCC), R37NS039518, 5P01NS072040 (CJW), 5F32NS076297 (IMC), FACS, microarrays at Boston Children's Hospital IDDRC facilities (NIH-P30-HD018655).

References

1. Medzhitov R. Origin and physiological roles of inflammation. Nature. 2008; 454:428–435. [PubMed: 18650913]
2. White RJ. Wound infection-associated pain. J Wound Care. 2009; 18:245–249. [PubMed: 19661848]
3. Ren K, Dubner R. Interactions between the immune and nervous systems in pain. Nat Med. 2010; 16:1267–1276. [PubMed: 20948535]
4. Miller LS, Cho JS. Immunity against Staphylococcus aureus cutaneous infections. Nat Rev Immunol. 2011; 11:505–518. [PubMed: 21720387]
5. Morgan M. Treatment of MRSA soft tissue infections: an overview. Injury. 2011; 42(Suppl 5):S11–17. [PubMed: 22196904]
6. Bubeck Wardenburg J, Patel RJ, Schneewind O. Surface proteins and exotoxins are required for the pathogenesis of Staphylococcus aureus pneumonia. Infect Immun. 2007; 75:1040–1044. [PubMed: 17101657]
7. Wang R, et al. Identification of novel cytolytic peptides as key virulence determinants for community-associated MRSA. Nat Med. 2007; 13:1510–1514. [PubMed: 17994102]

8. Gordon RJ, Lowy FD. Pathogenesis of methicillin-resistant Staphylococcus aureus infection. Clin Infect Dis. 2008; 46(Suppl 5):S350–359. [PubMed: 18462090]
9. Diep BA, et al. Complete genome sequence of USA300, an epidemic clone of community-acquired meticillin-resistant Staphylococcus aureus. Lancet. 2006; 367:731–739. [PubMed: 16517273]
10. Binshtok AM, et al. Nociceptors are interleukin-1beta sensors. J Neurosci. 2008; 28:14062–14073. [PubMed: 19109489]
11. Zhang XC, Kainz V, Burstein R, Levy D. Tumor necrosis factor-alpha induces sensitization of meningeal nociceptors mediated via local COX and p38 MAP kinase actions. Pain. 2011; 152:140–149. [PubMed: 21036476]
12. Muller-Anstett MA, et al. Staphylococcal peptidoglycan co-localizes with Nod2 and TLR2 and activates innate immune response via both receptors in primary murine keratinocytes. PLoS One. 2010; 5:e13153. [PubMed: 20949035]
13. Miller LS, et al. MyD88 mediates neutrophil recruitment initiated by IL-1R but not TLR2 activation in immunity against Staphylococcus aureus. Immunity. 2006; 24:79–91. [PubMed: 16413925]
14. Liu T, et al. Emerging roles of toll-like receptors in the control of pain and itch. Neurosci Bull. 2012; 28:133–44.
15. Diogenes A, et al. LPS sensitizes TRPV1 via activation of TLR4 in trigeminal sensory neurons. J Dent Res. 2011; 90:759–764. [PubMed: 21393555]
16. Rigby KM, DeLeo FR. Neutrophils in innate host defense against Staphylococcus aureus infections. Semin Immunopathol. 2011; 34:237–259. [PubMed: 22080185]
17. Rittner HL, et al. Mycobacteria attenuate nociceptive responses by formyl peptide receptor triggered opioid peptide release from neutrophils. PLoS Pathog. 2009; 5:e1000362. [PubMed: 19343210]
18. Shultz LD, et al. Human lymphoid and myeloid cell development in NOD/LtSz-scid IL2R gamma null mice engrafted with mobilized human hemopoietic stem cells. J Immunol. 2005; 174:6477–6489. [PubMed: 15879151]
19. Mombaerts P, et al. RAG-1-deficient mice have no mature B and T lymphocytes. Cell. 1992; 68:869–877. [PubMed: 1547488]
20. Agarwal N, Offermanns S, Kuner R. Conditional gene deletion in primary nociceptive neurons of trigeminal ganglia and dorsal root ganglia. Genesis. 2004; 38:122–129. [PubMed: 15048809]
21. Le Y, Murphy PM, Wang JM. Formyl-peptide receptors revisited. Trends in Immunology. 2002; 23:541–548. [PubMed: 12401407]
22. Liberles SD, et al. Formyl peptide receptors are candidate chemosensory receptors in the vomeronasal organ. Proc Natl Acad Sci USA. 2009; 106:9842–9847. [PubMed: 19497865]
23. Riviere S, Challet L, Fluegge D, Spehr M, Rodriguez I. Formyl peptide receptor-like proteins are a novel family of vomeronasal chemosensors. Nature. 2009; 459:574–577. [PubMed: 19387439]
24. Southgate EL, et al. Identification of formyl peptides from Listeria monocytogenes and Staphylococcus aureus as potent chemoattractants for mouse neutrophils. J Immunol. 2008; 181:1429–1437. [PubMed: 18606697]
25. Lennertz RC, Kossyreva EA, Smith AK, Stucky CL. TRPA1 mediates mechanical sensitization in nociceptors during inflammation. PLoS One. 2012; 7:e43597. [PubMed: 22927999]
26. Durr MC, et al. Neutrophil chemotaxis by pathogen-associated molecular patterns--formylated peptides are crucial but not the sole neutrophil attractants produced by Staphylococcus aureus. Cell Microbiol. 2006; 8:207–217. [PubMed: 16441432]
27. Inoshima I, et al. A Staphylococcus aureus pore-forming toxin subverts the activity of ADAM10 to cause lethal infection in mice. Nat Med. 2012; 17:1310–1314. [PubMed: 21926978]
28. Kennedy AD, et al. Targeting of alpha-hemolysin by active or passive immunization decreases severity of USA300 skin infection in a mouse model. J Infect Dis. 2010; 202:1050–1058. [PubMed: 20726702]
29. Dinges MM, Orwin PM, Schlievert PM. Exotoxins of Staphylococcus aureus. Clin Microbiol Rev. 2000; 13:16–34. table of contents. [PubMed: 10627489]

30. Wilke GA, Bubeck Wardenburg J. Role of a disintegrin and metalloprotease 10 in Staphylococcus aureus alpha-hemolysin-mediated cellular injury. Proc Natl Acad Sci U S A. 2010; 107:13473–13478. [PubMed: 20624979]
31. Chiu IM, von Hehn CA, Woolf CJ. Neurogenic inflammation and the peripheral nervous system in host defense and immunopathology. Nat Neurosci. 2012; 15:1063–1067. [PubMed: 22837035]
32. Abrahamsen B, et al. The cell and molecular basis of mechanical, cold, and inflammatory pain. Science. 2008; 321:702–705. [PubMed: 18669863]
33. McLachlan JB, et al. Mast cell-derived tumor necrosis factor induces hypertrophy of draining lymph nodes during infection. Nat Immunol. 2003; 4:1199–1205. [PubMed: 14595438]
34. Gautier EL, et al. Gene-expression profiles and transcriptional regulatory pathways that underlie the identity and diversity of mouse tissue macrophages. Nat Immunol. 2012; 13:1118–1128. [PubMed: 23023392]
35. Kim HK, Thammavongsa V, Schneewind O, Missiakas D. Recurrent infections and immune evasion strategies of Staphylococcus aureus. Curr Opin Microbiol. 2011; 15:92–99. [PubMed: 22088393]
36. Holzmann B. Modulation of immune responses by the neuropeptide CGRP. Amino Acids. 2011
37. Lang R, Kofler B. The galanin peptide family in inflammation. Neuropeptides. 2010; 45:1–8. [PubMed: 21087790]
38. Pinter E, Helyes Z, Szolcsanyi J. Inhibitory effect of somatostatin on inflammation and nociception. Pharmacol Ther. 2006; 112:440–456. [PubMed: 16764934]
39. Harzenetter MD, et al. Negative regulation of TLR responses by the neuropeptide CGRP is mediated by the transcriptional repressor ICER. J Immunol. 2007; 179:607–615. [PubMed: 17579082]
40. Gomes RN, et al. Calcitonin gene-related peptide inhibits local acute inflammation and protects mice against lethal endotoxemia. Shock. 2005; 24:590–594. [PubMed: 16317392]
41. Fernandes ES, et al. TRPV1 deletion enhances local inflammation and accelerates the onset of systemic inflammatory response syndrome. J Immunol. 2012; 188:5741–5751. [PubMed: 22547700]
42. Andersson U, Tracey KJ. Reflex principles of immunological homeostasis. Annu Rev Immunol. 2012; 30:313–335. [PubMed: 22224768]
43. Sun J, Singh V, Kajino-Sakamoto R, Aballay A. Neuronal GPCR controls innate immunity by regulating noncanonical unfolded protein response genes. Science. 2011; 332:729–732. [PubMed: 21474712]
44. Rosas-Ballina M, et al. Acetylcholine-synthesizing T cells relay neural signals in a vagus nerve circuit. Science. 2011; 334:98–101. [PubMed: 21921156]
45. Wong CH, Jenne CN, Lee WY, Leger C, Kubes P. Functional innervation of hepatic iNKT cells is immunosuppressive following stroke. Science. 2011; 334:101–105. [PubMed: 21921158]
46. Weihe E, et al. Molecular anatomy of the neuro-immune connection. Int J Neurosci. 1991; 59:1–23. [PubMed: 1774130]
47. Madisen L, et al. A robust and high-throughput Cre reporting and characterization system for the whole mouse brain. Nat Neurosci. 2009; 13:133–140. [PubMed: 20023653]
48. Voehringer D, et al. Homeostasis and effector function of lymphopenia-induced “memory-like” T cells in constitutively T cel-depleted mice. J Immunol. 2008; 180:4742–4753. [PubMed: 18354198]
49. Agarwal N, et al. Conditional gene deletion in primary nociceptive neurons. Lancet. 2006; 367:731–739. [PubMed: 16517273]
50. Pang YY, et al. agr-Dependent interactions of Staphylococcus aureus USA300 with human polymorphonuclear neutrophils. J Innate Immun. 2010; 2:546–559. [PubMed: 20829608]
51. Schenk S, Laddaga RA. Improved method for electroporation of Staphylococcus aures. FEMS Microbiol Lett. 1992; 73:133–138. [PubMed: 1521761]
52. Hill DR, et al. 2,2,2-Trifluoroethyl Fromate: a versatile and selective reagent for the formylation of alcohols, amines, and N-Hydroxylamines. Organic Letters. 2002; 4:111–113. [PubMed: 11772103]

53. Boxio R, et al. Mouse bone marrow contains large numbers of functionally competent neutrophils. J Leukoc Biol. 2004; 75:604–611. [PubMed: 14694182]

54. Sai J, et al. Parallel phosphatidylinositol 3-kinase (PI3K)-dependent and Src-dependent pathways lead to CXCL8-mediated Rac2 activation and chemotaxis. J Biol Chem. 2008; 283:26538–26547. [PubMed: 18662984]

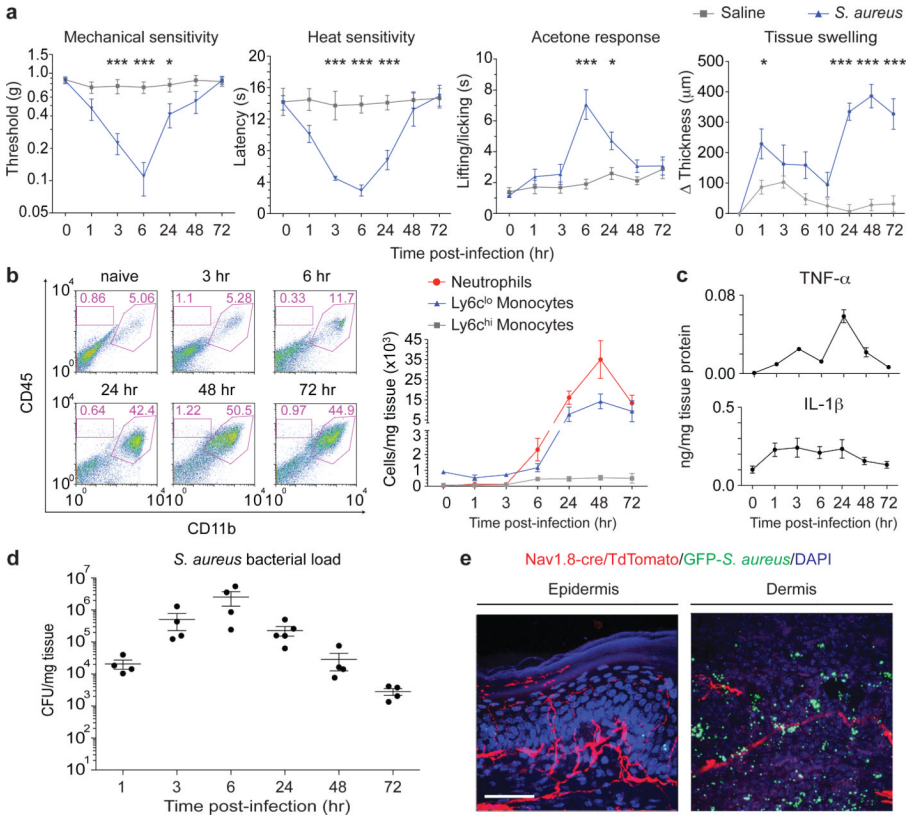

Figure 1. *S. aureus* infection induces pain hypersensitivity paralleling bacterial load but not immune activation

(a) *S. aureus* infection induces mechanical hypersensitivity (p=0.0021, n= 10/group), heat hypersensitivity (p<0.0001, n=10/group), acetone cold response (p<0.0001, n=20/group), and tissue swelling (p<0.0001, n=10/group). *p<0.05, ***p<0.001. **(b)** Left, flow cytometry shows myeloid ($CD11b^+CD45^+$) but not lymphoid ($CD11b^-CD45^+$) immune expansion in infected tissues. Right, Quantification of infected tissue neutrophils ($CD11b^+Ly6G^+$), $Ly6c^{hi}$ monocytes ($CD11b^+Ly6G^-Ly6C^{hi}$), and $Ly6C^{lo}$ monocytes/macrophages ($CD11b^+Ly6G^-Ly6C^{lo}$). n=3/time-point. **(c)** TNF-α, IL-1β levels in infected tissues. n=4/time-point. **(d)** Bacterial load recovery. n=4/time-point. **(e)** GFP-*S. aureus* are in proximity with Nav1.8-Cre/$TdTomato^+$ dermal nerve fibers, 3 hours post-infection. Scalebar,100 μm. Error bars, mean±s.e.m.

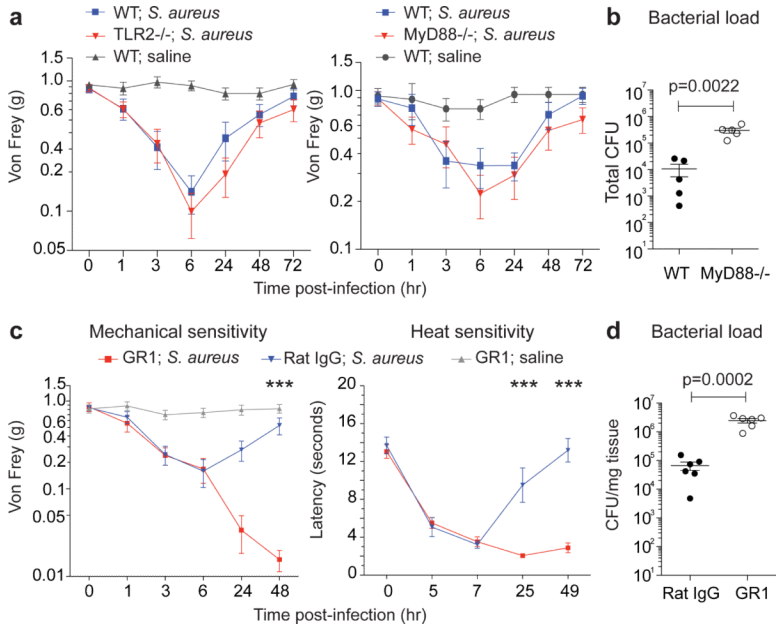

Figure 2. Innate immunity through TLR2/MyD88 and neutrophils/monocytes is not necessary for pain during *S. aureus* infection

(a) Infection-induced mechanical hypersensitivity is similar in TLR2$^{-/-}$ mice (n=10 infected) compared to WT mice (n=10 infected, n=10 saline injected) (p=0.744), and MyD88$^{-/-}$ mice (n=10 infected) relative to WT mice (n=11 infected, n=7 saline injected) (p=0.533). **(b)** Bacterial load, 3 days post-infection (n=5 each). **(c)** Infection-induced mechanical (p<0.0001) and heat (p<0.0001) hypersensitivity are increased in GR1 treated mice (n=10 infected, n=10 saline) compared to rat IgG treated mice (n=10 infected). Bonferroni, ***p<0.001. **(d)** Bacterial load, 2 days post-infection (n=6 each). Error bars, mean±s.e.m.

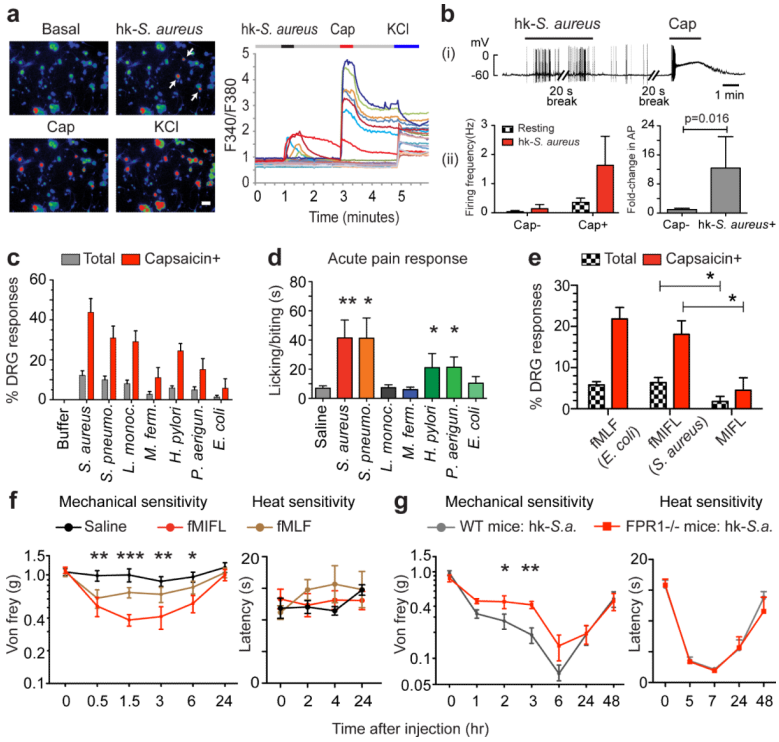

Figure 3. Bacterial heat-stable components including N-formylated peptides activate nociceptors

(a) Hk-*S. aureus* induces calcium flux in capsaicin, KCl responsive DRG neurons (arrows, traces). **(b)** (i) Representative recording, (ii) firing frequency upon hk-*S. aureus* application (5 capsaicin-responsive cells, 9 unresponsive). **(c)** DRG responsive proportions to hk-bacteria (n=4-26 fields/condition). **(d)** Acute pain induction: saline (n=13), hk-*S. aureus* (n=12), hk-*S. pneumonia* (n=14), hk-*L. monocytogenes* (n=5), hk-*M. fermentans* (n=6), hk-*H. pylori* (n=5), hk-*P. aeruginosa* (n=8), hk-*E. coli* (n=6). **p<0.01, *p<0.05. **(e)** DRG responsive proportions to formyl peptides (n=3-14 fields/condition). **(f-g)** fMLF, fMIFL injection induces mechanical hypersensitivity. $Fpr1^{-/-}$ mice show reduced hk-*S. aureus* mechanical hypersensitivity (p=0.0089). fMIFL vs. saline, $Fpr1^{-/-}$ vs. WT: *p<0.05; **p<0.01; ***p<0.001. Error bars, mean±s.e.m.

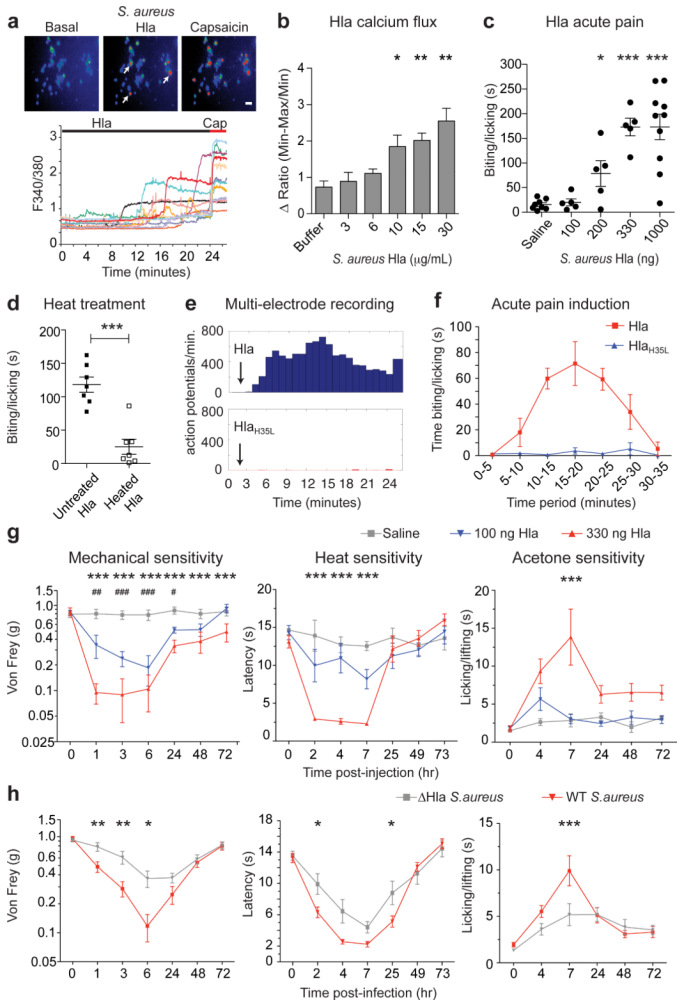

Figure 4. Heat-sensitive *S. aureus* Hla activates nociceptors and contributes to infection-induced hyperalgesia

(a) Hla application evoked DRG neuron calcium flux (arrows, traces), **(b-c)** dose-dependent calcium flux (n=3/condition) and acute pain (n=5-10/group). *p<0.05, ***p<0.001. **(d)** Heat pre-treatment abolishes Hla-induced pain (1 μg, n=7/group). **(e)** Hla, HLA_{H35L} evoked DRG neuron action potentials (arrow, Hla application, n=3/condition). **(f)** Hla (1 μg, n=6) but not Hla_{H35L} (1 μg, n=5) induced acute pain. **(g)** Hla 100 ng (n=8), 330 ng (n=8), saline (n=8) injection induced hypersensitivity. 100 ng vs. saline: ***p<0.001; 330 ng vs. saline: #p<0.05, ##p<0.01, ###p<0.001. **(h)** *S. aureus* lacking Hla (n=12) produced less mechanical (p=0.0056), heat (p=0.0193), acetone (p=0.0118) hypersensitivity than WT *S. aureus* (n=13). *p<0.05; **p<0.01; ***p<0.001. Error bars, mean±s.e.m.

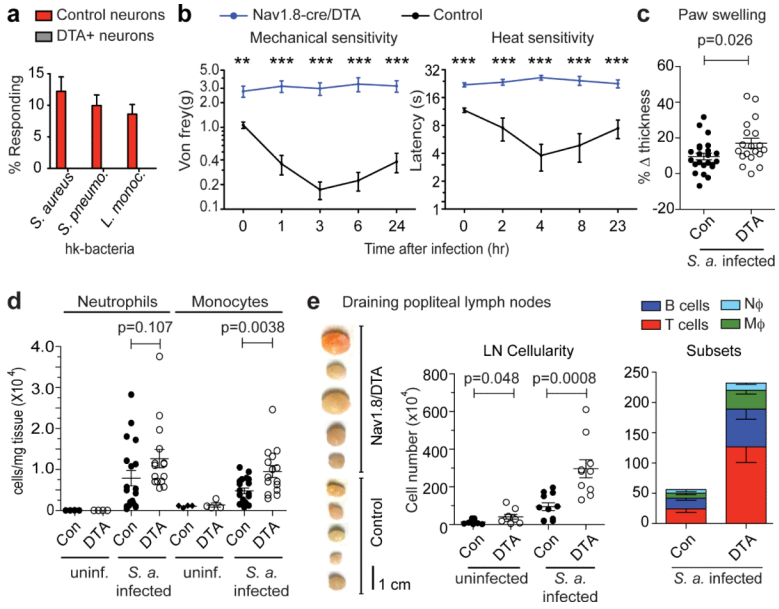

Figure 5. Nociceptor ablation leads to increased local inflammation and lymphadenopathy following *S. aureus* infection

(a) Nav1.8-Cre/DTA neurons lack hk-bacteria responses. **(b)** Infection-induced mechanical (p=0.0027), heat hypersensitivity (p=0.0003) in Nav1.8-Cre/DTA mice (n=10 mechanical, n=6 heat) and Control littermates (n=12 mechanical, n=6 heat). ***p<0.001. **(c-e)** Parameters analyzed 24 hours post-infection. **(c)** Tissue swelling: Nav1.8-Cre/DTA (n=23), Control (n=19). **(d)** Plantar neutrophils/monocytes: Nav1.8-Cre/DTA: n=4 uninfected, n=15 infected; Control: n=4 uninfected, n=19 infected. **(e)** Popliteal lymph node images (infected), lymph node cellularity (Nav1.8-Cre/DTA: n=9 uninfected, n=10 infected; Control: n=9 uninfected, n=11 infected), and lymph node monocyte/macrophage (Mφ), neutrophil (Nφ), T, B cell subsets (n=5 each). Error bars, mean±s.e.m.

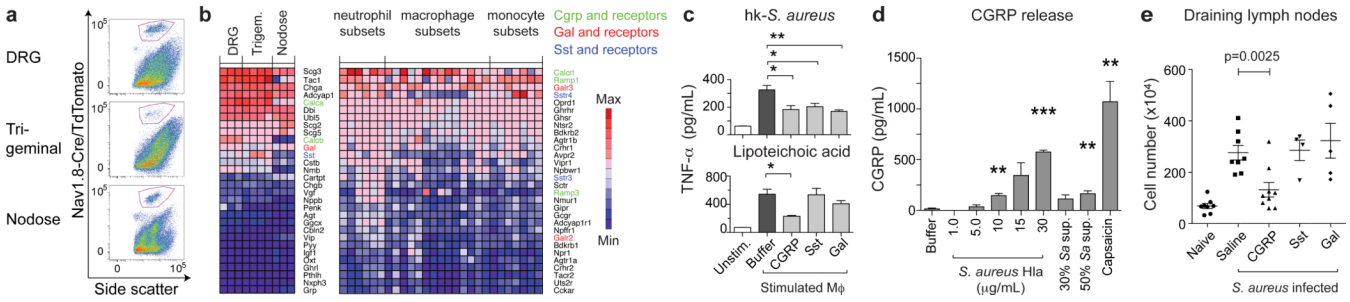

Figure 6. Nociceptor derived neuropeptides regulate innate immune activation

(a) Nav1.8-Cre/TdTomato^{+} DRG, trigeminal, nodose ganglia neurons were purified by flow cytometry (gates shown). **(b)** Top 30 nociceptor-expressed neuropeptides and myeloid immune cell-expressed neuropeptide receptors, shown from maximum to minimum. **(c)** Hla, *S. aureus* supernatant, and capsaicin (100 nM) induce DRG neuron CGRP release. **p<0.01; ***p<0.001. **(d)** TNF-α production by hk-*S. aureus* or Lipoteichoic acid stimulated macrophages was suppressed by CGRP, Sst, Gal (neuropeptide concentrations, 1 μM; *p<0.05). **(e)** CGRP injection decreased lymphadenopathy 24 hours post-*S. aureus* infection. Error bars, mean±s.e.m.